Late Holocene environmental changes reconstructed from stable isotope and geochemical records from a cushion-plant peatland in the Chilean Central Andes (27°S)

S.T. Kock[1,2], K. Schittek[2], B. Mächtle[2], H. Wissel[1], A. Maldonado[3,4,5] and A. Lücke[1]

[1] Institute of Bio- and Geosciences, Agrosphere Institute (IBG-3), Forschungszentrum Jülich GmbH, Germany

[2] Institute of Geography, Heidelberg Center for the Environment (HCE), Heidelberg University, Germany

[3] Centro de Estudios Avanzados en Zonas Áridas (CEAZA), La Serena, Chile

[4] Instituto de Investigación Multidisciplinar en Ciencia y Tecnología, Universidad de La Serena

[5] Departamento de Biología Marina, Universidad Católica del Norte, Coquimbo, Chile

Correspondence to: S.T. Kock (s.kock@uni-heidelberg.de)

Abstract

A Late Holocene paleoenvironmental record was obtained from the Lagunillas cushion peatland (LP, 27°12' S, 69°17' W), located in the dry Puna of the western Central Andes. Ten radiocarbon dates build the chronology for the last 1800 cal a BP. Analyses of stable isotopes on cellulose ($\delta^{18}O_{cell}$, $\delta^{13}C_{cell}$) and geochemical proxies on organic matter ($\delta^{13}C_{OM}$, $\delta^{15}N_{OM}$, TOC, TN, LOI, T_{535}) were conducted to identify major paleoenvironmental changes in this record. Simultaneously, ambient water ($\delta^{18}O$, $\delta^{2}H$) and plant samples of the dominant species *Oxychloe andina* ($\delta^{18}O_{cell}$, $\delta^{13}C_{cell}$) reveal insights into modern conditions. The record evinces distinct multi-centennial oscillations of peat layer thickness and $\delta^{18}O_{cell}$. Decomposition, changes in the dominating plant species as well as in plant parts (leaves/roots) can be excluded as driving factors for this oscillations. Thus, $\delta^{18}O_{cell}$ seems to be externally forced and reflects humidity changes. Accordingly, around 470 cal a BP a distinct change towards increased humidity occurred, lasting during the LIA until about 70 cal a BP. Humid conditions prevailed between 1530 and 1270 cal a BP. Increasing $\delta^{18}O_{cell}$ values since -30 cal a BP mark a trend towards again increased aridity.

KEYWORDS: cushion peatlands; Central Andes; stable isotopes; cellulose; Late Holocene

1 Introduction

Paleoenvironmental studies covering the past two millennia have increased significantly within the last years aiming to improve the spatial coverage of paleoclimate proxy data and to evaluate climate and earth system models (PAGES 2k Consortium, 2017). However, both tasks often lack continuous and reliable climate records from extreme environmental locations (Flantua *et al*., 2016). Like the highlands of the Central Andes of South America those are characterized by steep altitudinal gradients and harsh environmental conditions like low temperatures, high solar radiation, low oxygen content and a reduced availability of water (Körner, 2007) and comprise only a limited number of paleoclimatic records (Villalba *et al*., 2009). However, due to their function as climatic barrier for the South American continent, the Central Andes represent a key region for the understanding of the interplay between the two major atmospheric circulation systems, the South American summer monsoon (SASM) and the Southern Hemisphere westerly winds (SHW) (Garreaud *et al*., 2003).

High-Andean cushion-plant peatlands can be reliable archives for paleoenvironmental investigations in the Central Andes, because these soligeneous peatlands are distributed near biological and hydrological limits for plant growth (Schittek *et al*., 2012; Squeo *et al*., 2006). They respond sensitive to climatic changes and anthropogenic disturbances (Schittek, 2014) and are able to fill gaps in paleoenvironmental data coverage. In contrast to the cushion-plant peatlands of the eastern Central Andes (e.g. Schittek *et al*., 2016), those of the western Central Andes are usually characterized by a highly heterogenic stratigraphy, i.e. their peat layers are frequently interspersed with layers of clastic material (e.g. Earle *et al*., 2003).

Stable isotope analyses are a well-established tool in paleoecological investigations of Northern Hemisphere peatlands (Ménot-Combes *et al*., 2002; Moschen *et al*., 2009). In contrast to the Northern Hemisphere peat-accumulating moss genus *Sphagnum*, the high-Andean cushion-forming peat accumulators are vascular plants. Additional to their dependence on the isotopic source value of the precursor molecules (water, carbon dioxide), vascular plants are able to regulate their gas exchange by stomata. During metabolic processes, isotope fractionation processes occur and lead to further changes in oxygen ($\delta^{18}O$) and carbon isotope ($\delta^{13}C$) composition of plant tissue (Ménot and Burns, 2001).

Previous isotopic studies on cushion-plant peatlands in South America have been conducted in Bolivia (Gouze *et al*., 1987) and Peru (*Distichia* peatlands; Engel *et al*., 2014; Skrzypek *et al*., 2011). Other investigations on vascular plants in peatlands are known from Switzerland

(Ménot and Burns, 2001), China (Hong *et al*., 2009, 2000) and New Zealand (Amesbury *et al*., 2015a, 2015b). Oxygen isotopes are very often applied within paleoecological investigations (e.g. Ménot-Combes *et al*., 2002). The $\delta^{18}O$ value of plant cellulose is directly related to the respective leaf water ($\delta^{18}O_{LW}$) and enriched by about 27.0 ‰ due to biochemical fraction during formation of primary photosynthates (glucose) (Sternberg, 2009; DeNiro and Epstein, 1979). The aperture of plant stomata has a high influence on $\delta^{18}O_{LW}$. Stomatal closure, caused for example by drought conditions, could lead to a decrease of stomatal conductance and increased enrichment of $\delta^{18}O_{LW}$ values during transpiration (Farquhar *et al*., 2007). Due to their dependence on the respective water source value ($\delta^{18}O_{SW}$) and leaf water enrichment, reported $\delta^{18}O$ values for extracted cellulose of vascular plants in peatlands cover a considerable range (Amesbury *et al*., 2015b; Hong *et al*., 2009).

For carbon isotopes, a relationship between $\delta^{13}C$ and temperature (Amesbury *et al*., 2015a; Engel *et al*., 2014; Skrzypek *et al*., 2011; Ménot and Burns, 2001) was reported. However, Ménot and Burns (2001) also found that on an altitudinal gradient the atmospheric CO_2 concentration is a stronger determinant for $\delta^{13}C$ values of peat plants than temperature. Amesbury *et al*. (2015b) used $\delta^{18}O$ for tracking precipitation moisture sources, while Hong *et al*. (2009, 2000) interpret $\delta^{18}O$ as a proxy for surface air temperature changes. Therefore, reliable interpretation of plant isotopic compositions needs prior information about metabolic processes as well as knowledge about the site-specific climatological setup and asks for a multiproxy investigation.

Here, we investigate the organic-rich peat sections of a four meter core of the Lagunillas peatland (LP) and complement this data set with investigations of local ambient water and plant samples. We analysed the elemental composition of carbon (TOC) and nitrogen (TN), loss on ignition (LOI) and humification values (T_{535}), together with the carbon and total nitrogen isotope composition of bulk peat and plant organic matter (OM) and carbon and oxygen isotope composition of cellulose of core samples. Our main goals were (1) to study the context for $\delta^{18}O$ and $\delta^{13}C$ values of cushion peatlands to provide useful paleoclimatic proxies despite the heterogeneous stratigraphy as being typical for the peatlands in the western Central Andes and (2) to derive knowledge on centennial scale variations of the hydrologic conditions at the investigated peatland.

2 The study area

The Lagunillas cushion peatland (LP, 27°12’ S, W 69°17’ W, 3823 m a.s.l.) is located in the Cordillera Principal de los Andes in the Chilean province Copiapó (Figure 1). It is an extended high-altitude peatland within the valley of Quebrada Lagunitas, covering a length of 9 kilometer between 4075 and 3770 m a.s.l.. Adjacent to the Argentine border, the LP is situated on the southernmost margin of the Altiplano-Puna Plateau, embedded between the borders of the Parque Nacional Nevado de Tres Cruces in the north, east and south. The study area is dominated by dry valleys (Quebradas) filled with colluvial clastics, mostly in form of gravel, and rocky scree slopes that are underlain by Miocene volcanic andesits (Iriarte *et al*., 1998).

Located at the southwestern margin of the Arid Diagonal, annual averaged precipitation sums do not exceed 150-200 mm (Iriarte *et al*., 1998; Aravena, 1995), consisting of both tropical summer and extratropical winter precipitation. However, exact precipitation amounts remain unknown due to a high distance to and the distinct lower altitude of the next meteorological station (Pastos Grande, 27° 06’ S, 69° 33’ W, 2260 m a.s.l.), where higher extratropical precipitation values can be expected. During austral summer, the weakening of the meridional temperature gradient causes a southward displacement of the subtropical jet stream (ITCZ), while deep convection over the central part of the continent starts to develop, together leading to the monsoon-like climate of central South America (e.g. Garreaud and Aceituno, 2007; Hastenrath, 1997). Moisture provided by the South American Summer Monsoon (SASM) reaches the study area mostly in form of grail, locally known as the ‘Bolivian winter’ phenomenon (Juliá *et al.*, 2008). Wintertime precipitation can be divided into cold-front snowfall- and cut-off patterns. Cold front-events lead to a northward displacement of cold polar air masses and mainly influence the western range of the Andes. Cut off–events are characterized by polar air that has been cut off from the westerly circulation and drifting northwards as an isolated cell. In combination with warmer tropical air masses, clouds can be formed leading to precipitation, mostly in form of snow (Vuille and Ammann, 1997).

The regional potential evapotranspiration exceeds modern precipitation amounts by a factor of 5, up to 1000 mm/year (Risacher *et al*., 1999; Hastenrath and Kutzbach, 1985) and up to 66% of the precipitation is lost due to sublimation (Vuille and Ammann, 1997), which is why the study area is arid, offering year-round moisture only along rare spring-fed rivulets.

The LP is situated within a V-shaped valley of an ephemeral stream with relatively steep slopes. Below an adjacent high-Andean lake at 4072 m a.s.l. in the upper part of the peatland, the juncaceous cushion plants are interspersed with shallow pools that are connected by superficial water flows, originating from springs. The modern peatland vegetation around the coring site (3825 m a.s.l.) is dominated by the main cushion-forming species *Oxychloe andina* (*O. andina*), partially interspersed with *Zameioscirpus atacamensis, Deyeuxia curvula* and *Deyeuxia velutina*. In heavily degraded areas, caused by grazing of ungulates, *Carex gayana*-dominated turfs are formed, which are very poor in species.

Compared to peatland areas at higher altitudes within the valley, the surface of the investigated part is characterized by the absence of interspersed shallow pools due to a natural drainage by a gully, locally called arroyo (Figure 2). This gully incised into the peatland in the late 1950's probably formed by increased runoff after higher precipitation amounts in the study area and/or intensified grazing activity (Kock *et al.*, accepted).

3 Material and Methods

3.1 Field survey, sampling and chronology

During fieldwork in March 2016, the core C1581 with a total length of four meters was extracted in one-meter segments by percussion coring (Wacker vibra-corer). Furthermore, various ambient plant samples of the dominant peat forming species (*O. andina*) were taken in a close radius around the coring point as well as several water samples of the complete LP. In the laboratory, the ambient plant samples of *O. andina* were separated in leaves and rhizomes and washed repeatedly with deionized water to remove clastic material. The core was opened lengthwise with a modified core saw, cut into two halves, photographed and described lithologically. The caving material, detected by comparing the stratigraphy of a parallel core (see Kock *et al*., accepted, for details), was excluded for the development of the final undisturbed core profile. All depths mentioned in the text are profile depth, and thus after the removal of caving material. The first core half, except layers dominated by sandy or coarse clastic material without organic matter, was cut in one-centimeter slices from which boundary areas were removed to exclude potential contamination. The peat samples were used for cellulose extraction (see 3.3). Accordingly, the second half was prepared in 1 cm slices for stable isotope analyses ($\delta^{13}C$, $\delta^{15}N$), element content analyses as well as loss on ignition (LOI) and humification (T_{535}) measurements on bulk material. Loss on ignition was determined every second centimeter and the humification index every fourth centimeter.. The organic-rich sediment sections with TOC values >4.5%, thus >9% organic material due to the approximation based on our measurements of $LOI_{550°}$ = TOC*1.959, will be called peat sections in the following.

Samples for radiocarbon dating were chosen near the upper and lower boundaries of major peat layers to generate a consistent internal age control for the respective peat sections and to provide information about the temporal duration of interspersed clastic material accumulation. Additionally, one sample was extracted from close below the surface of the extinct peat deposit (see Figure 2) to date the incision of the peatland. Bulk peat material of 0.5-1.0 cm^3 was taken from the selected samples for radiocarbon dating by Accelerator Mass Spectrometry (AMS) at the Poznan Radiocarbon Laboratory (Poznan, Poland) (Table S1).

Radiocarbon ages were calibrated using CALIB 7.0.4 (Stuiver *et al*., 2013) with the SHCal13 data set for Southern Hemisphere calibration (Hogg *et al*., 2013). To calibrate modern

radiocarbon dates, CALIBomb (Reimer *et al*., 2004) was used. The MCAgeDepth software package was used to develop the age-depth model based on ten radiocarbon dates. The age-depth model is calculated as the median of 800 Monte Carlo approaches to generate confidence intervals integrating the probabilistic nature of calibrated ^{14}C-dates. The software computed a cubic smoothing spline through all dates where the significance of each date in the fitted spline depends on its standard deviation (Higuera *et al*., 2009). All discussed ages are calibrated ages BP (cal a BP), if not mentioned otherwise.

Pearson correlation coefficients ($p > 0.05$) were determined by using the R software (version 3.2.2) and the package "rioja" (version 0.9-15; Juggins, 2017) to describe parameter relations.

3.2 Water samples

Stable isotope analysis was carried out using a Cavity Ringdown Spectrometer (L2130-I, Picarro). Results are reported as δ values relative to Vienna Standard Mean Ocean Water (VSMOW) (Gonfiantini, 1978). Internal standards, calibrated against VSMOW, Standard Light Antarctic Precipitation, and Greenland Ice Sheet Precipitation were used to ensure long-term stability of analyses. The precision of the analytical system was ≤ 0.1‰ for $\delta^{18}O$ and ≤ 1.0‰ for $\delta^{2}H$.

3.3 Core and modern plant samples

Cellulose extraction of the core samples is based on a slightly advanced protocol following Wissel *et al*. (2008). Prior to the protocol, bulk peat samples were separated into three size fractions by sieving at 200 µm and 1000 µm, after two hours of initial treatment with NaOH (5%) to ensure dispersion and repeated washing with deionized water (~20°C). Cellulose extraction was conducted for all peat samples of the size fraction 200-1000 µm, down to a depth of 81 cm for the size fraction >1000 µm due to lack of material afterwards and in total for 8 samples of the size fraction <200 for reasons of comparison (see chapter 4.1).

For $\delta^{18}O_{cell}$ analyses, about 275 µg of freeze-dried cellulose was weighed in silver capsules, crimped and stored for at least 24 h in a vacuum drier at 100°C before analyses. Samples were then pyrolysed at 1450°C by using a high temperature pyrolysis analyzer (HT-O, HEKAtech) and measured on-line with a coupled isotope ratio mass spectrometry (IRMS) (Isoprime, GV Instruments) to determine the oxygen stable isotope ratio. The $\delta^{13}C_{cell}$ values were determined using 200-300µg of dried cellulose weighed into tin foil cups. Samples were combusted at

1080°C using an element analyzer (EuroEA, Eurovector) interfaced on-line to an isotope IRMS (Isoprime, GV Instruments).

The bulk samples of the second core half as well as the modern plant samples, separated into leaves and rhizomes, were freeze-dried and milled (Retsch, MM 400). Organic matter stable isotopes of carbon ($\delta^{13}C_{OM}$) and carbon content (TOC) as well as nitrogen isotopes ($\delta^{15}N_{OM}$) and nitrogen content (TN) were measured separately. Samples were analyzed via combustion as described above. Pyrolysis as described above was also used for organic matter stable oxygen isotope analyses ($\delta^{18}O_{OM}$) of plant samples.

All isotope results are presented as δ-values [‰] according to the equation

$$\delta = (R_S/R_{St} - 1) \bullet 1000$$

where R_S is the isotope ratio of the sample ($D/^1H$, $^{13}C/^{12}C$, $^{15}N/^{14}N$, $^{18}O/^{16}O$) and R_{St} is the isotope ratio of the respective standard. Calibrated laboratory standards were used to control the quality of the analyses and to relate the raw values to the isotopic reference scales (VSMOW for hydrogen and oxygen, VPDB for carbon, AIR for nitrogen). The overall precision of replicate analyses is estimated to be better than 5% (rel.) for carbon and oxygen content, <0.1‰ for $\delta^{15}N$ and $\delta^{13}C$ and <0.25‰ for $\delta^{18}O$.

Loss on ignition (LOI) determination followed standard procedures after Heiri *et al*. (2001) with an initial milled material weight of 25-30 mg. Humification measurements followed the procedures recommended by Blackford & Chambers (1993) and Chambers *et al.* (2011), based on a target value of 20 mg organic matter in the sample.

4 Results

4.1 Stratigraphy and chronology

The stratigraphy of core C1581 is characterized by changes between homogeneous, faintly layered peat and clastic material, mostly dominated by sand and gravel components (Figure 3a and b). Kock *et al.* (accepted) could demonstrate that the clastic sediments reflect changes in the geomorphodynamics within the study area. These depositions can either be explained by strong, single precipitation events, triggering high amounts of sediment, or repeated smaller erosional events with respectively lower amounts of clastic material, however, without sufficient recovery time for cushion plants to regrow.

Within the first 83 cm, the peat sections (0-11 cm, 16-33 cm, 43-64) are interspersed with sand and silt dominated facies (11-16 cm, 33-43 cm, 64-83 cm), while between 83 cm and 226 cm, layers of peat (83–103.5 cm, 120.5-145.5 cm, 176.5-197.5 cm) alternate with gravel-dominated facies (103.5-120.5 cm, 145.5-176.5 cm). From 226 cm to 278 cm, the stratigraphy is characterized by a very heterogeneous layering with more frequent changes between different clastic grainsizes, only interrupted by a peat section between 231-255 cm. Between 278 cm and 308.5 cm, the facies is dominated by gravel, followed mainly by peat layers down to 357.5 cm. This peat section is interspersed with a layer of sand and silt between 314.5 and 318.5 cm, and further, a layer of gravel between 343.5 and 350.5 cm.

In total, 15 bulk peat samples (Table S1) were retrieved close to the boundaries of major peat layers to generate a consistent internal age control for the respective peat sections . Five samples were excluded from the age depth model. Their radiocarbon ages indicated contamination with old carbon, most likely from reworking, or reveal too young carbon without visible signs for caving, probably due to root contamination. The developed age depth model (Figure 3c) provides modelled ages for each sample depth and shows different sedimentation rates and changing temporal resolutions for the investigated peat sections.

4.2 Modern data

Modern water samples show a large scatter in $\delta^{18}O$ and $\delta^{2}H$ values within the altitudinal range of the LP between 3822 and 4072 m a.s.l. (Table S2). Overall, $\delta^{18}O$ values scatter between -11.4‰ and -2.9‰, while the $\delta^{2}H$ values vary between -87.4‰ and -50.8‰. The data reveal a very good correlation between $\delta^{18}O$ and $\delta^{2}H$ ($r = 0.99$).

The analysis of different plant parts of *O. andina* from the LP reveals distinct differences between leaves and rhizomes (Table 1). The organic matter isotope data indicate that leaves are enriched in ^{18}O and ^{13}C compared to rhizomes. The isotopic difference is larger for $\delta^{18}O_{OM}$ values (2.5‰) than for $\delta^{13}C_{OM}$ (0.8‰). Comparable $\delta^{13}C$ values of modern plants were reported by Earle *et al*. (2003) for *O. andina* (-24.3‰ ±0.6‰) and by Arroyo *et al*. (1990) for vascular plants in Chile between 3200 and 4500 m a.s.l. (-25.8‰ ±1.5‰).

4.3 Core data

4.3.1 Inter-peat-section variability

We examined all organic peat layers with identifiable accumulation of *O. andina*-peat. This resulted in the investigation of 15 distinct layers with variable thickness based on the mean values of centimeter wide samples (Table 2).

The arithmetic mean values of the proxy records exhibit noticeable variations between the distinct peat layers. TOC values show a striking variability between 4.8% and 30.1%, while LOI values range between 13.3% and 59.9%. Further differences can be noticed in the cellulose yields, ranging from 4.4% to 12.9%. T_{535} values exhibit lower differences, however, show a decreasing trend with increasing depth. This is comparable to the TOC/TN values that also show a low variability and decreasing ratios with depth. Similar characteristics could be found in $\delta^{13}C_{OM}$ and $\delta^{13}C_{cell}$ values, with constantly more enriched $\delta^{13}C_{cell}$ values. $\delta^{18}O_{cell}$ values exhibit strong variations, ranging from 26.5% to 30.6‰.

4.3.2 Intra-peat-section variability

The high-resolution dataset (Figure 4) reveals additional information about the intra-peat-section variability of the record.

For several proxies, a considerably higher variability occurs within the upper meter of the profile. Especially TOC (between 4.8% and 38.3%, second section) and LOI (between 14.4% and 75.2%, second section) values reveal high differences within single peat sections. Furthermore, a slightly negative trend is visible in the TOC/TN values within the upper 100 cm, while $\delta^{13}C_{OM}$ show a tendency towards more enriched values. Towards the oldest sections of the record, the values show lower frequencies of changes without distinct trends. Humification values show low variabilities with slightly higher values in the uppermost, and, vice versa, slightly lower values in the lowest two sections of the core.

Besides the superimposed fluctuations described earlier, $\delta^{18}O_{cell}$ data also reveal medium intra-section variability of up to 4‰ (e.g. third peat layer, see Table 2). Cellulose yields reveal low to medium fluctuations (max. 12.8%, third peat layer) with an overall slight decreasing trend. The values of $\delta^{13}C_{cell}$ show a strong enrichment within the first 40 cm, but level out thereafter. Compared to $\delta^{13}C_{OM}$ values, $\delta^{13}C_{cell}$ values are enriched by about ~3‰, which is comparable with the results of Ménot and Burns (2001) for vascular plants, and further, with Moschen *et al.* (2009) for *Sphagnum* peatlands.

Pearson correlation coefficients (Table S3) reveal highly significant correlations between LOI and TOC ($r=0.99$, $p<0.01$), between TN and TOC ($r=0.99$, $p<0.01$) and between TN and LOI ($r = 0.98$, $p<0.01$). T_{535} reveal strong negative correlations with $\delta^{13}C_{cell}$ ($r=-0.66$, $p<0.01$ for fraction 200-1000µm) and $\delta^{13}C_{OM}$ ($r=-0.59$, $p<0.01$), while positive correlations exist with TOC/TN ($r=0.47$, $p=0.01$) and cellulose yield ($r=0.37$, $p=0.08$). The similarity between

$\delta^{13}C_{cell}$ and $\delta^{13}C_{OM}$ is confirmed by high correlation coefficients of $r=0.63$ ($p<0.01$). $\delta^{18}O_{cell}$ values only show weak negative correlation with the cellulose yield ($r=-0.36$, $p<0.01$).

5 Discussion

5.1 Modern hydrology and plant composition

The isotopic composition of modern water samples gives an insight into the present hydrological system of LP. Presumably, the springs are fed by groundwater of recent precipitation periods instead of deeper, fossil waters, thus, isotopic source values of the peatland's water are directly linked to the isotope composition of local precipitation. However, local evaporation processes of the open waters and during infiltration may have additional influence.

Lowest δ^2H and $\delta^{18}O$ values are observed in the water of a spring and of the stream water close to the coring location and can give an approximation of the isotopic composition of meteoric water infiltrating into the LP (for details see Table S2). Medium values occur in interspersed shallow pools that are only temporally interconnected by superficial channels. However, they have a reduced surface compared to their water bodies and can be affected by evaporation. Highest δ^2H and $\delta^{18}O$ values occur in samples from the adjacent lake in the uppermost part of the peatland, which is characterized by a relatively shallow water depth (between 2 and 3 m) and a large surface (~6.000 m²), thus, is susceptible for strong evaporation effects.

The isotopic composition of the LP water samples (Figure 5) are compared with the Global Meteoric Water Line (GMWL) due to insufficient data for the development of a Local Meteoric Water Line. The data reveal a linear relation and define a regression line between δ^2H and $\delta^{18}O$ values ($\delta^2H = 4.30\ \delta^{18}O - 38.64$) that can be interpreted as local evaporation line (LEL). The slope of the LEL is comparable to those of other evaporating surface waters in the Central Andes (e.g. Mook *et al*., 2001). We interpret the existing of a well described LEL as evidence for a well mixed meteoric water source (precipitation) for the LP (Strauch *et al*., 2009). Thus, we expect a close connection of the LP to the meteoric water cycle without effective delay effects or contributions of old groundwater, which is potentially different in isotope composition.

The plant samples (Table 1) reveal distinct isotopic differences between leaves and rhizomes of *O. andina* for $\delta^{18}O$ ($\Delta\ \delta^{18}O_{l\text{-}r} = 2.51‰$). Compared to other vascular plants of peatlands

like *Empodisma*, this difference is low (~Δ $\delta^{18}O_{l\text{-}r}$ = 8.4‰ to 11.8‰, Amesbury *et al.*, 2015b). As the composition of the residual peat is a mixture of leaves and rhizomes, we suggest that changes of compositions have negligible effects on the $\delta^{18}O$ values of the extracted cellulose from core samples. Even a complete but unlikely transition from a composition of only leaves to only rhizomes could not explain differences of 6.8‰ within the record. The differences of $\delta^{13}C$ between leaves and rhizomes ($\Delta\ \delta^{13}C_{l\text{-}r}$ = 0.77‰) are comparable to other studies on vascular plants in peatlands (~Δ $\delta^{13}C_{l\text{-}r}$ = 0.85‰ to 1.25‰, Amesbury *et al.*, 2015a). As with the $\delta^{18}O$ values, even a complete change of the peat composition could not explain a total variation of 3.9‰ $\delta^{13}C$ within the record.

Taking the spring water value (Table S2) as best known approximation for the source water value, the $\delta^{18}O_{cell}$ of the first peat section indicates ^{18}O enrichment of 40.3 ‰. Thus, leaf water enrichment is considerably strong.

5.2 Oxygen isotope variations of the Lagunillas peatland record

The most prominent feature of the Lagunillas record is the explicit multi-centennial oscillation of the $\delta^{18}O_{cell}$ values (Figure 6). Based on our knowledge from ambient data, we already excluded changing contributions from rhizomes to leaves as the source for the $\delta^{18}O_{cell}$ change that might have been induced by preferential preservation. Accordingly and similarly, major changes in peat degradation and preservation can be excluded on a broader scale as peat humification remains comparably constant. Furthermore, the indicator for humification T_{535} is uncorrelated with the $\delta^{18}O_{cell}$ record in contrast to negative correlations occurring for $\delta^{13}C_{cell}$ and $\delta^{13}C_{OM}$. Despite huge variations in TOC, among others affected by dilution effects, results of macrofossil analysis with regard to changes in plant species (results not shown) argue against major changes in the Lagunillas peatland vegetation assemblage that otherwise could have potentially explained the observed changes in $\delta^{18}O_{cell}$.

Transpiration has the potential to cause large variations in the oxygen stable isotope composition of assimilates, finally transferred to cellulose, as stomatal aperture is a major factor governing leaf water isotope enrichment in vascular plants (Offermann *et al.*, 2011). Given the extreme environmental conditions for plant growth at LP and the cushion growth habit generating specific ‘canopy-like’ humidity and turbulence conditions for the cushion plants, limited effective changes in stomatal aperture seem plausible (despite the general

diurnal and seasonal oscillations). As water-use efficiency of C3 plants show correlations with the isotopic composition of plant carbon (Farquhar and Richards, 1984), we take the missing correlation between both $\delta^{13}C$ records and the $\delta^{18}O_{cell}$ record as a supporting argument for a limited impact of leaf water evaporative enrichment on the $\delta^{18}O_{cell}$ values. Rather, we expect evaporative enrichment to be a standing, but not highly fluctuating factor on a longer-term basis (e.g. weeks to growth periods) for the LP, i.e. not to be the leading variable for $\delta^{18}O_{cell}$ variations. Thus, we deduce that the observed multi-centennial oscillation of $\delta^{18}O_{cell}$ is externally forced.

The depleted $\delta^{18}O_{cell}$ values are closely connected to increased layer thickness and further, to increased and high TOC concentrations, although no direct connection between TOC and oxygen cellulose isotope values exist. This excludes clastic input as the main driver for the thickness increase of the respective sections, indicating improved plant growth in the peatland as the driving factor for the increased layer thickness. In view of the environmental setting where water availability obviously is the limiting factor for plant growth, we conclude that water availability, and thus precipitation, must have considerably increased around 470 cal a BP at LP. Interestingly, a connection between increasing amounts and decreasing oxygen isotope composition of precipitation in our study area can be explained by the SASM (e.g. Vuille *et al.*, 2012) as well by the SHW circulation system (Valero-Garcés *et al.*, 2005 IAEA/WMO, 2004). The SASM isotopic signature is mainly influenced by the rainout upstream along the long-range transport of the moisture from the tropical Atlantic across the Amazon basin to the Andes (e.g. Bustamante *et al.*, 2016). A stronger SASM can be associated with more depleted ^{18}O values of the summer precipitation (e.g. Vuille & Werner, 2005). The SHW induced winter precipitation originates from the Pacific and shows comparable tendencies in the oxygen isotope signature with lower values during higher precipitation amounts, as it is visible in the GNIP database (IAEA/WMO, 2004).

5.3 Supporting evidence for moisture changes after 470 cal a BP

During the last 1800 years, the $\delta^{18}O_{cell}$ record reveals three major changes in moisture conditions at the Lagunillas peatland (27° S). We here compare the LP record with other sensitive paleoclimatic records of South America from north to south (18-35° S) and at different longitudes (66-70° W) (Figure 7).

Visibly, the most distinct change in the LP record occurred around 470 cal a BP with a shift towards strongly depleted ^{18}O values (Figure 7a). This period lasted until around 70 cal a BP, thus occurred contemporaneous with the prominent Little Ice Age (LIA) period. According to the austral summer temperature reconstruction for the high Andes of Central Chile by de Jong *et al*. (2013, Figure 7d), this period seems to be characterized by higher temperatures compared to the period before 470 cal a BP. As argued above, strongly depleted $^{18}O_{cell}$ values at Lagunillas indicate increased precipitation amounts, independent of the atmospheric source of meteoric water. Thus, lower $^{18}O_{cell}$ values reflect higher humidity, which cannot be allocated to a certain source (SASM, SHW) presently. However, distinct changes during that time could be found in various climate archives like lake sediments, tree-rings, glaciers and cushion peatlands. Precipitation reconstruction for the Altiplano of Bolivia and Northern Chile (18-22° S, 66-69° W, SASM influenced) based on tree-ring width series of *Polylepis tarapacana* revealed partly increased precipitation amounts after 490 cal a BP (Morales *et al*., 2012, Figure 7b). However, over centennial timescales the record reveals no clear oscillation. In accordance with our record, high Mn/Fe ratios of the Cerro Tuzgle cushion peatland, located in the Puna of northwest Argentina (24° S, 67° W, SASM influenced), indicated increasing humidity between 300 and 100 cal a BP (Schittek *et al*., 2016, Figure 7c). Investigations on the extension of glacier moraines in the Andes of Argentina (34-35° S, 70° W, SASM & SHW influenced) revealed that the LIA maximum occurred between 400 and 230 cal a BP with a glacier re-advance starting around 120 cal a BP (Espizua & Pitte, 2009). On the other hand, reduced Poaceae percentages from Laguna Chepical, located in the high Andes of Central Chile (32° S, 70 W, SHW influenced), point toward drier conditions during the LIA (Martel-Cea *et al.* 2016).

Another distinct phase with lower $\delta^{18}O_{cell}$ values in our record occurs between 1530 and 1270 cal a BP, indicating wetter conditions at the LP. Slightly increased humidity during that time is also evident e.g. in the Cerro Tuzgle Peatland (Schittek *et al*., 2016). It remains elusive if again increasing $\delta^{18}O_{cell}$ values in the up permost peat section (since around -30 cal a BP / 1980 AD) mark a trend towards increased aridity. However, Vuille *et al*. (2003) found a trend toward decreased precipitation in the southern tropical Andes during the 20th century, based on available climate station data.

This suggests that our interpretation of wetter conditions at the LP during the LIA is plausible, even though timing and extent vary due to the sensitivity of the different proxy-data and the longitudinal expression (18-35 °S) of the paleoclimate archives. Moreover, the regional

comparison suggests a stronger SASM during that time (e.g Vuille *et al*., 2012), while the SHW influence seems to be reduced (e.g. Martel-Cea *et al.* 2016).

6 Conclusion

The investigated Lagunillas cushion peatland, located in the western Central Andes, resolves paleoenvironmental conditions of the past 1800 years. Despite its heterogeneous stratigraphy with an intercalation of organic and inorganic sediment layers, the record provides important paleoenvironmental information for an area, which is characterized by a low frequency of climate archives. Most of the investigated organic-rich (peat) sections possess temporal resolution of up to 2 a/cm^{-1}, thus also bear further potential for high-resolution paleoclimate reconstruction.

We argue that $\delta^{18}O_{cell}$ values are a suitable proxy for moisture conditions at the LP reflecting local humidity changes. The LEL of the ambient water samples indicates that old groundwater with a potentially different isotopically composition does not affect the hydrology of the peatland and thus suggests a close connection of the LP to the meteoric water cycle. Although the record reveals slight changes in decomposition (T_{535}) values between 91.5 and 83 %; TOC/TN values between 11.4 and 17.2%), no effect on the $\delta^{18}O_{cell}$ can be determined. Accordingly and similarly, changes in the dominating plant species as well as in plant part composition ($\Delta^{18}O_{l\text{-}r} = 2.51$) can be excluded as potential factor of influence. The observed multi-centennial oscillation of $\delta^{18}O_{cell}$ seems to be externally forced, thus, reflects changes in humidity at the LP caused by changes in precipitation amount and source region.

Most distinct changes occur around 470 cal a BP with an increase in precipitation in the study area, lasting until 70 cal a BP, covering the LIA period. Several sensitive paleoclimate records across the Andes of South America (between 18-35°S) confirm increasing precipitation during that time, supporting our interpretation. Another phase of low $\delta^{18}O_{cell}$ values also indicates wetter conditions in the study area between 1530 and 1270 cal a BP. Furthermore, a trend towards increasing aridity is visible since -30 cal a BP. Further studies on comparable cushion peatlands in the region are necessary to substantiate and generalize our argument with regard to $\delta^{18}O_{cell}$ as local/regional moisture indicator and the origin of the moisture source (SASM, SHW). Our results demonstrate the potential residing in this type of cushion peat archive as recorders of paleoenvironmental changes in the Central Andes.

Data accessibility

Multiproxy data from Lagunillas Peatland will be made available via the National Oceanic and Atmospheric Administration (NOAA) Paleoclimate database.

Supplementary information

Table S1. Radiocarbon ages of core C1581 from the LP**.**

Table S2. Stable isotope values of ambient water samples.

Table S3. Pearson correlation coefficients (r) between geochemical and isotopic proxies of core C1581 based on the full data set.

Acknowledgements. We acknowledge support from the German Science Foundation (DFG) priority research program SPP-1803 "EarhShape: Earth Surface Shaping by Biota" (grants Ma 4504/1-1 to BM and Schi 1366/1-1 to KS). We are grateful to the Chilean National Park Service (CONAF) for providing access to the sample locations and on-site support of our research. The authors give their sincere thanks to Ulrike Langen and Josip Sučić for their commitment in the laboratory. Furthermore, we acknowledge the support of Eugenia de Porras for all the help during the field campaign.

References

Amesbury MJ, Charman DJ, Newnham RM *et al*. 2015a. Carbon stable isotopes as a palaeoclimate proxy in vascular plant dominated peatlands. *Geochimica et Cosmochimica Acta* **164**: 161-174.

Amesbury MJ, Charman DJ, Newnham RM *et al.* 2015b. Can oxygen stable isotopes be used to track precipitation moisture source in vascular plant-dominated peatlands? *Earth and Planetary Science Letters* **430**: 149-159.

Aravena R. 1995. Isotope hydrology and geochemistry of northern Chile ground waters. *Bulletin de l'Institute Français de Ètudes Andines* **24**: 495-503.

Arroyo MK, Medina E, Ziegler H. 1990. Distribution and $\delta^{13}C$ values of Portulacaceae species of the high Andes in northern Chile. *Plant Biology* **103(**3): 291-295.

Blackford JJ, Chambers FM. 1993. Determining the degree of peat decomposition for peat based palaeoclimatic studies. *International Peat Journal* **5**: 7–24.

Bustamante MG, Cruz FW, Vuille M *et al*. 2005. Holocene changes in monsoon precipitation in the Andes of NE Peru based on $\delta^{18}O$ speleothem records. *Quaternary Science Reviews* **146**: 274-287.

Chambers FM, Beilman DW, Yu Z. 2011. Methods for determining peat humification and for quantifying peat bulk density, organic matter and carbon content for palaeostudies of climate and peatland carbon dynamics. *Mires and Peat* **7**(7): 1-10.

de Jong R, von Gunten L, Maldonado A *et al*. 2013. Late Holocene summer temperatures in the central Andes reconstructed from the sediments of high-elevation Laguna Chepical, Chile (32°S). *Climate of the Past* **9**: 1921–1932.

DeNiro MJ, Epstein S. 1981. Isotopic composition of cellulose from aquatic organisms. *Geochimica et Cosmochimica Acta* **45**(10): 1885-1894.

Earle LR, Warner BG, Aravena R. 2003. Rapid development of an unusual peat-accumulating ecosystem in the Chilean Altiplano. *Quaternary Research* **59**: 2-11.

Engel Z, Skrzypek G, Chuman T *et al*. 2014. Climate in the Western Cordillera of the Central Andes over the last 4300 years. *Quaternary Science Reviews* **99**: 60-77.

Espizua LE, Pitte P. 2009. The Little Ice Age glacier advance in the Central Andes (35°S), Argentina. *Palaeogeography, Palaeoclimatology, Palaeoecology* **281**: 345–350.

Farquhar GD, Richards RA. 1984. Isotopic composition of plant carbon correlates with water-use efficiency of wheat genotypes. *Functional Plant Biology* **11**(6): 539-552.

Farquhar GD, Cernusak LA, Barnes B. 2007. Heavy water fractionation during transpiration. *Plant Physiology* **143**(1): 11-18.

Flantua SGA, Hooghiemstra H, Vuille M *et al*. 2016. Climate variability and human impact in South America during the last 2000 years: synthesis and perspectives from pollen records. *Climate of the Past* **12**: 483-523.

Garreaud R, Vuille M, Clement AC. 2003. The climate of the Altiplano: observed current conditions and mechanisms of past changes. *Palaeogeography, palaeoclimatology, palaeoecology* **194**(1-3): 5-22.

Garreaud RD, Aceituno P. 2007. Atmospheric Circulation and Climatic Variability. In *The Physcial Geography of South America*, Veblen TT, Young KR, Orme AR (eds). Oxford University Press: Oxford; 45–59.

Gonfiantini R. 1978. Standards for stable isotope measurements in natural compounds. *Nature* **271**: 534-536.

Gouze P, Ferhi A, Fontes JC *et al*. 1987. Composition isotopique (18 O) de la matière organique des tourbières actuelles et holocènes en Bolivie: résultats préliminaires et perspectives d'application en paléoclimatologie. *Géodynamique* **2**(2): 113-116.

Hastenrath S, Kutzbach J. 1985. Late Pleistocene climate and water budget of the South American Altiplano. *Quaternary Research* **24**(3): 249-256.

Hastenrath S. 1997. Annual cycle of upper air circulation and convective activity over the tropical Americas. *Journal of Geophysical Research* **102**(D4): 4627 – 4274.

Heiri O, Lotter AF, Lemcke G. 2001. Loss on ignition as a method for estimating organic and carbonate content in sediments: reproducibility and comparability of results. *Journal of paleolimnology* **25**(1): 101-110.

Higuera PE, Brubaker LB, Anderson PM *et al*. 2009. Vegetation mediated the impacts of postglacial climate change on fire regimes in the south-central Brooks Range, Alaska. *Ecological Monographs* **79**(2): 201–219.

Hogg AG, Quan H, Blackwell PG *et al*. 2013. SHCAL13 southern hemisphere calibration, 0-50,000 years cal BP. *Radiocarbon* **55**(4): 1889-1903.

Hong YT, Jiang HB, Liu TS *et al*. 2000. Response of climate to solar forcing recorded in a 6000-year $\delta^{18}O$ time-series of Chinese peat cellulose. *The Holocene* **10**(1): 1–7.

Hong YT, Hong B, Lin QH *et al*. 2009. Synchronous climate anomalies in the western North Pacific and North Atlantic regions during the last 14000 years. *Quaternary Science Reviews* **28** (9): 840–849.

IAEA/WMO. 2004. Global Network of Isotopes in Precipitation. GNIP Database. https://nucleus.iaea.org/wiser/index.php [12. December 2017]

Iriarte S, Ugalde I, Venegas, M. 1998. Hidrogeologia de la cuenca Laguna del Negro Francisco (Region de Atacarma). SERNAGEOMIN document de trabajo 10: Santiago de Chile.

Juggins S. 2015. Rioja: Analysis of Quaternary Science Data, R package version (0.9-9). https://cran.r-project.org/web/packages/rioja/index.html [04. February 2018]

Juliá C, Montecinos S, Maldonado A. 2008. Características Climáticas de la Región de Atacama. In *Libro Rojo de la Flora Nativa y de los Sitios Prioritarios para su Conservación: Región de Atacama*, Squeo FA, Arancio G, Gutiérrez JR (eds). Ediciones Universidad de La Serena: La Serena; 25-42.

Kock S, Schittek K, Lücke A *et al*. accepted. Geomorphodynamics of the western Chilean Central Andes (27°S) during the last 1800 cal. yr BP as recorded in a high-Andean cushion peatland. *Zeitschrift für Geomorphologie*.

Körner, C. 2007. The use of 'altitude' in ecological research. *Trends in ecology & evolution* **22**(11): 569-574.

Martel-Cea A, Maldonado A, Grosjean M *et al*. 2016. Late Holocene environmental changes as recorded in the sediments of high Andean Laguna Chepical, Central Chile (32°S; 3050 m a.s.l.). *Palaeogeography, Palaeoclimatology, Palaeoecology* **461**: 44–54.

Ménot G, Burns, SJ. 2001. Carbon isotopes in ombrogenic peat bog plants as climatic indicators: calibration from an altitudinal transect in Switzerland. *Organic Geochemistry* **32**(2): 233-245.

Ménot-Combes G, Burns SJ, Leuenberger M. 2002. Variations of $^{18}O/^{16}O$ in plants from temperate peat bogs (Switzerland): implications for paleoclimatic studies. *Earth and Planetary Science Letters* **202**(2): 419-434.

Mook, WG. 2001. Environmental isotopes in the hydrological cycle: Principles and applications. Vol 1. Introduction, Theory, methods, review. UNESCO – IAEA: Paris.

Morales MS, Christie DA, Villalba R *et al*. 2012. Precipitation changes in the South American Altiplano since 1300 AD reconstructed by tree-rings. *Climate of the Past* **8**: 653-666.

Moschen R, Kühl N, Rehberger I *et al*. 2009. Stable carbon and oxygen isotopes in sub-fossil Sphagnum: Assessment of their applicability for palaeoclimatology. *Chemical Geology* **259**(3): 262-272.

Offermann C, Ferrio JP, Holst J *et al*. 2011. The long way down—are carbon and oxygen isotope signals in the tree ring uncoupled from canopy physiological processes? *Tree Physiology* **31**(10): 1088–1102.

PAGES2K Consortium 2017. A global multiproxy database for temperature reconstructions of the Common Era. *Scientific data* **4**: 170088.

Reimer PJ, Brown TA, Reimer RW. 2004. Discussion: reporting and calibration of post-bomb ^{14}C data. *Radiocarbon* **46**(3): 1299-1304.

Risacher F, Alonso H, Salazar C. 1999. Geoquímica de aguas en cuencas cerradas: I, II y III regions – Chile/Volumen I Sintesis. Ministerio de Obras Públicas: Santiago de Chile.

Schittek K, Forbriger M, Schäbitz F *et al*. 2012. Cushion Peatlands – Fragile Water Resources in the High Andes of Southern Peru. In *Water – Contributions to Sustainable Supply and Use, Landscape and Sustainable Development*, Weingartner H, Blumenstein O, Vavelidis M. (eds.). Workinggroup Landscape and Sustainable Development: Salzburg; 63–84.

Schittek K. 2014. Cushion peatlands in the high Andes of northwest Argentina as archives for paleoenvironmental research. Dissertationes Botanicae 412, J. Cramer in der Gebrüder Borntraeger Verlagsbuchhandlung: Stuttgart.

Schittek K, Kock ST, Lücke A *et al*. 2016. A high-altitude peatland record of environmental changes in the NW Argentine Andes (24°S) over the last 2100 years. *Climate of the Past* **12**: 1165–1180.

Skrzypek G, Engel Z, Chuman T *et al*. 2011. Distichia peat – A new stable isotope paleoclimate proxy for the Andes. *Earth and Planetary Science Letters* **307**(3): 298-308.

Squeo FA, Warner BG, Aravena R *et al*. 2006. Bofedales: high altitude peatlands of the central Andes. *Revista chilena de historia natural* **79**(2): 245-255.

Sternberg LDSLO. 2009. Oxygen stable isotope ratios of tree-ring cellulose: the next phase of understanding. *New Phytologist* **181**(3): 553-562.

Strauch G, Oyarzún R, Reinstorf F *et al.* 2009. Interaction of water components in the semi-arid Huasco and Limarí river basins, North Central Chile. *Advances in Geosciences **22***: 51-57.Stuiver M, Reimer PJ, Reimer RW. 2013. Calib 7.0. Radiocarbon calibration program. http://calib.org/calib/download/calib704.zip [12 January 2018]

Valero-Garcés BL, Jenny B, Rondanelli M *et al*. 2005. Palaeohydrology of Laguna de Tagua Tagua (34 30′ S) and moisture fluctuations in Central Chile for the last 46 000 yr. *Journal of Quaternary Science* **20**(7-8): 625-641.

Villalba R, Grosjean M, Kiefer T. 2009. Long-term multi-proxy climate reconstructions and dynamics in South America (LOTRED-SA): state of the art and perspectives. *Palaeogeography, Palaeoclimatology, Palaeoecology* **281**(3-4): 175-179.

Vuille M. Ammann C. 1997. Regional snowfall patterns in the high, arid Andes. *Climatic Change* **36**: 413-423.

Vuille M., Bradley RS, Werner M *et al*. 2003. 20th century climate change in the tropical Andes: observations and model results. In *Climate variability and change in high elevation regions: Past, present & future*, Diaz HF (ed.). Springer: Dordrecht; 75-99.

Vuille M, Werner M. 2005. Stable isotopes in precipitation recording South American summer monsoon and ENSO variability: observations and model results. *Climate dynamics* **25**(4): 401-413.

Vuille M, Burns SJ, Taylor BL *et al*. 2012. A review of the South American monsoon history as recorded in stable isotopic proxies over the past two millennia. *Climate of the Past* **8**: 1309–1321.

Wissel H, Mayr C, Lücke A. 2008. A new approach for the isolation of cellulose from aquatic plant tissue and freshwater sediments for stable isotope analysis. *Organic Geochemistry* **39**(11): 1545-1561.

Table 1. OM isotope values of ambient plant samples from the LP. Given are number of samples (n) mean $\delta^{18}O$ and $\delta^{13}C$ values of OM together with standard deviation (SD) and the mean isotopic difference between leaves and rhizomes ($\Delta\ \delta^{18}O_{l\text{-}r}$, $\Delta\ \delta^{13}C_{l\text{-}r}$).

Plant sample		**n**	**$\delta^{18}O$ [‰] VSMOW**	**SD**	**n**	**$\delta^{13}C$ [‰] VPDB**	**SD**	**$\Delta^{18}O_{l\text{-}r}$**	**$\Delta^{13}C_{l\text{-}r}$**
Oxychloe andina	leaves	19	26.52	0.86	9	-24.94	0.49	2.51	0.77
	rhizomes	21	24.01	1.10	34	-25.68	0.56		

Table 2. Characterization of distinct organic-rich sediment layers (peat) of the Lagunillas cushion peatland with the respective arithmetic mean values (bold) and standard deviations (in brackets) of bulk material and cellulose (fraction 200-1000 µm). Given are total organic carbon content (TOC), bulk stable organic carbon isotope composition ($\delta^{13}C_{bulk}$), total nitrogen content (TN), total stable nitrogen isotope composition ($\delta^{15}N$), TOC/TN ratio, loss on ignition (LOI_{550}), humification index (T_{535}), cellulose stable oxygen composition ($\delta^{18}O_{cell}$) cellulose stable carbon isotope composition ($\delta^{13}C_{cell}$) and cellulose yield (yield). Layer number in stratigraphical order (section), core depth of layer (depth), number of samples in layer respectively layer thickness (n) and mean temporal resolution of centimeter samples in layer (res.).

section	depth [cm]	n	res.	TOC [%]	$\delta^{13}C_{OM}$ VPDB [‰]	TN [%]	$\delta^{15}N_{OM}$ AIR [‰]	TOC/TN	LOI [%]	T_{535} [%]	$\delta^{18}O_{cell}$ VSMOW [‰]	$\delta^{13}C_{cell}$ VPDB [‰]	yield [%]
1	0-11	**11**	3.6	**30.1** (±5.9)	**-26.6** (±0.5)	**2.0** (±0.3)	**4.2** (±1.7)	**15.0** (±1.0)	**59.3** (±14.6)	**90.2** (±1.0)	**28.9** (±1.0)	**-24.9** (±0.7)	**9.4** (±1.6)
2	16-33	**17**	3.1	**20.6** (±12.7)	**-26.0** (±0.4)	**1.4** (±0.8)	**6.7** (±0.4)	**14.0** (±0.8)	**40.3** (±25.6)	**86.5** (±1.2)	**27.6** (±1.0)	**-23.3** (±0.4)	**6.3** (±2.4)
3	43-64	**21**	2.1	**21.7** (±10.5)	**-25.8** (±0.5)	**1.4** (±0.6)	**6.6** (±0.8)	**14.8** (±1.3)	**46.3** (±19.6)	**86.3** (±0.5)	**27.2** (±1.1)	**-23.2** (±0.5)	**12.9** (±4.7)
4	80-103.5	**23**	4.4	**17.1** (±5.9)	**-25.7** (±0.6)	**1.3** (±0.4)	**5.9** (±0.8)	**13.4** (±1.1)	**38.4** (±14.0)	**87.3** (±0.6)	**26.5** (±1.1)	**-22.7** (±0.3)	**10.1** (±2.7)
5	119.5-136.5	**17**	5.3	**6.4** (±3.5)	**-25.6** (±0.4)	**0.5** (±0.3)	**6.1** (±0.4)	**12.5** (±0.3)	**13.3** (±6.3)	**86.7** (±0.3)	**26.9** (±0.7)	**-22.8** (±0.3)	**6.5** (±2.8)
6	140.5-144.5	4	4.2	**7.7** (±0.9)	**-26.4** (±0.2)	**0.6** (±0.1)	**5.8** (±0.3)	**13.3** (±0.3)	**22.2** (±0.4)	**86.6** (±0.0)	**27.4** (±0.4)	**-23.4** (±0.2)	**5.8** (±2.4)
7	176.5-197.5	**21**	2.6	**22.6** (±6.8)	**-25.2** (±0.4)	**1.7** (±0.5)	**5.8** (±1.3)	**13.1** (±0.7)	**46.0** (±13.4)	**85.6** (±0.3)	**29.3** (±0.5)	**-22.8** (±0.2)	**6.7** (±1.4)
8	231-235	4	4.5	**12.8** (±6.5)	**-25.8** (±0.3)	**0.9** (±0.4)	**5.1** (±0.5)	**14.9** (±0.5)	**24.4** (±3.4)	**88.0** (±0.0)	**30.5** (±0.7)	**-23.0** (±0.3)	**7.1** (±0.6)
9	238-240	2	4.4	**4.8** (±3.2)	**-25.8** (±0.1)	**0.4** (±0.2)	**4.6** (±0.6)	**13.5** (±0.1)	**18.4** (±0.0)	**86.5** (±0.0)	**30.3** (±1.0)	**-22.8** (±0.4)	**5.2** (±1.0)
10	243-255	**12**	4.1	**14.9** (±7.3)	**-25.6** (±0.1)	**1.1** (±0.5)	**5.2** (±1.2)	**13.8** (±0.7)	**34.0** (±15.3)	**86.8** (±0.0)	**29.5** (±0.7)	**-23.2** (±0.1)	**8.1** (±1.5)
11	275-279	4	6.9	**13.5** (±9.9)	**-25.7** (±0.5)	**0.9** (±0.7)	**3.1** (±0.5)	**13.8** (±1.0)	**30.4** (±16.5)	**86.6** (±0.0)	**29.5** (±0.7)	**-23.2** (±0.2)	**6.9** (±0.9)
12	308.5-315.5	**7**	10.8	**13.9** (±6.8)	**-26.6** (±0.3)	**1.1** (±0.6)	**5.7** (±0.7)	**12.9** (±0.6)	**30.4** (±13.2)	/	**28.7** (±0.3)	**-23.1** (±0.3)	**6.2** (±1.7)
13	318.5 - 334.5	**16**	10.5	**19.5** (±7.1)	**-25.8** (±0.6)	**1.5** (±0.6)	**5.7** (±0.7)	**13.5** (±0.8)	**42.0** (±15.5)	**85.3** (±3.9)	**28.0** (±0.5)	**-23.0** (±0.5)	**7.4** (±1.5)
14	336.5-343.5	**7**	10.2	**14.5** (±5.8)	**-25.6** (±0.3)	**1.2** (±0.5)	**6.5** (±0.5)	**12.6** (±0.3)	**43.0†** (±2.1)	**84.1** (±0.1)	**30.6** (±0.4)	**-23.1** (±0.2)	**4.4** (±1.0)
15	350.5-357.5	**7**	10.1	**15.2** (±5.5)	**-25.8** (±0.3)	**1.3** (±0.4)	**5.7** (±0.7)	**11.9** (±0.3)	**32.0** (±13.0)	**83.5** (±0.0)	**30.1** (±0.5)	**-23.0** (±0.1)	**4.7†**(±1.1)

† *one outlier removed*

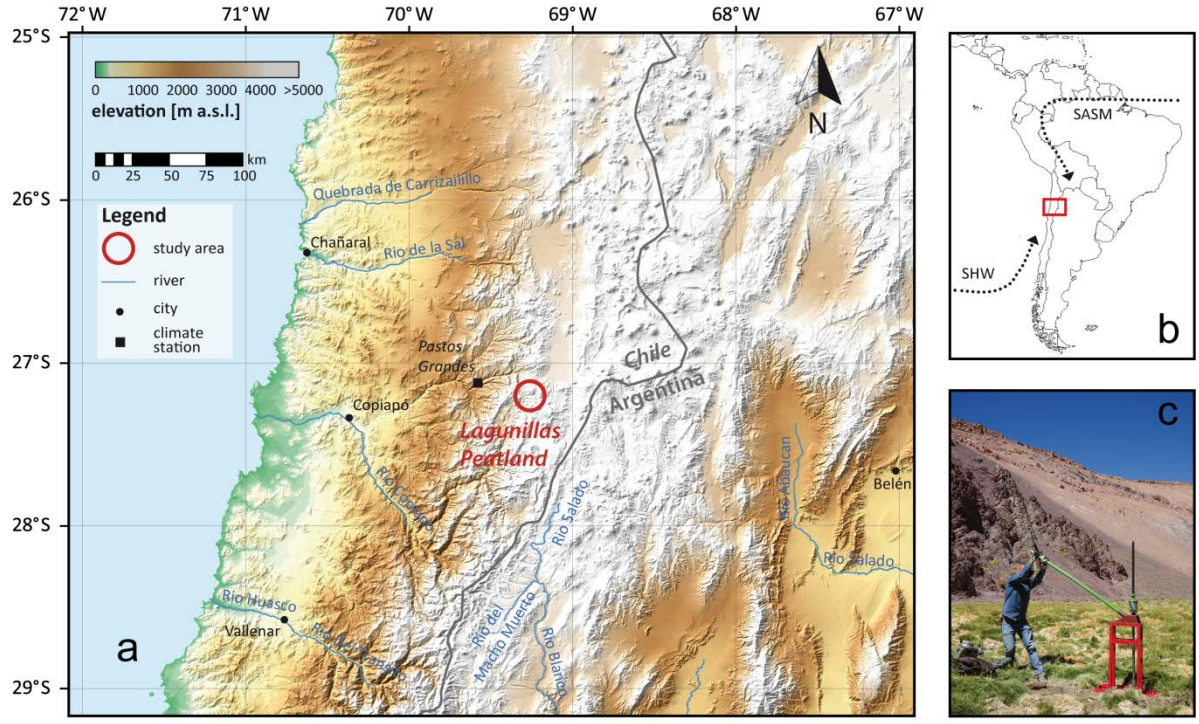

Figure 1. Regional setting of the Lagunillas peatland. (a) Location of the study area in the Western Central Andes of Chile close to the Argentine border (data source: DGM-GTOPO 30). Climate station Pastos Grandes (27°06'S, 69°33'W, 2260 m a.s.l.) is marked as a black square. (b) Map of South America indicating the climatic moisture sources (South American summer monsoon (SASM) and Southern Hemisphere Westerlies (SHW)) to the study area, with a red box showing the map section visible in (a) (data source: GLCF World Data). (c) Picture of the coring location in the investigated part of Lagunillas peatland facing in NW direction.

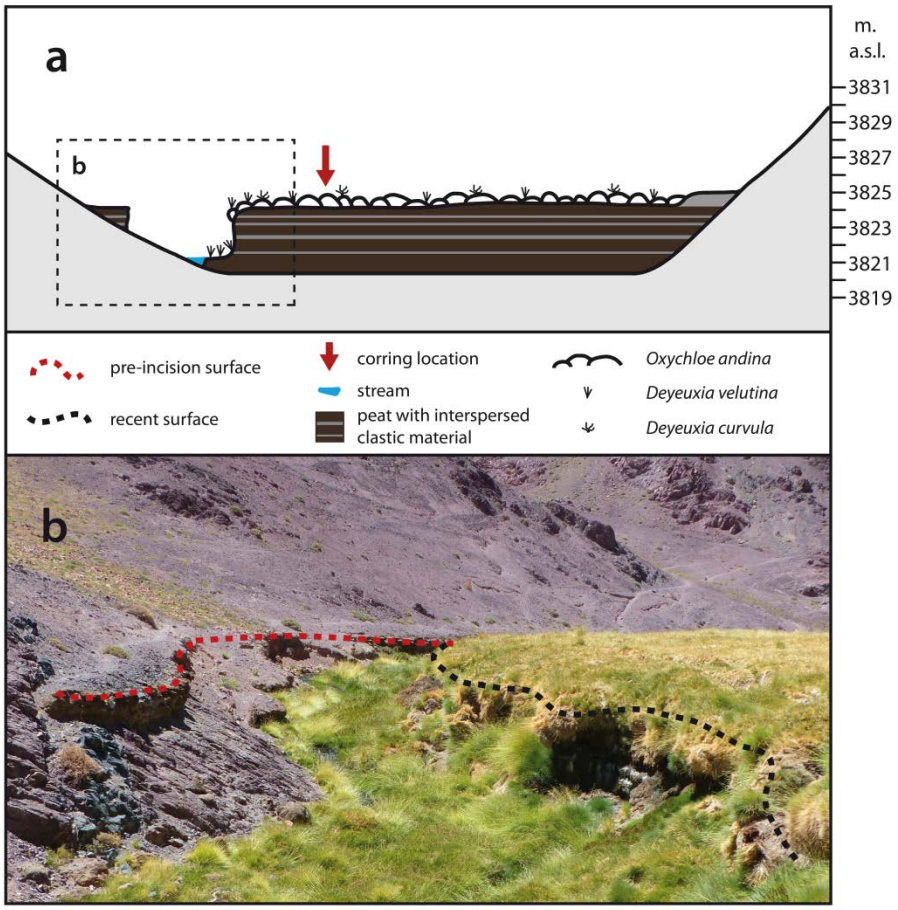

Figure 2. Gully incision of the peat-body at LP. (a) Schematic cross-section of the investigated part of the LP, showing the recent peatland's floral composition, the stratigraphy of the underlying peat as well as the gully incision. (b) Close-up of the gully incision, view towards the NE direction. The dotted lines indicate the former (red; extinct peat deposit on the slope) and recent (black) surface respectively.

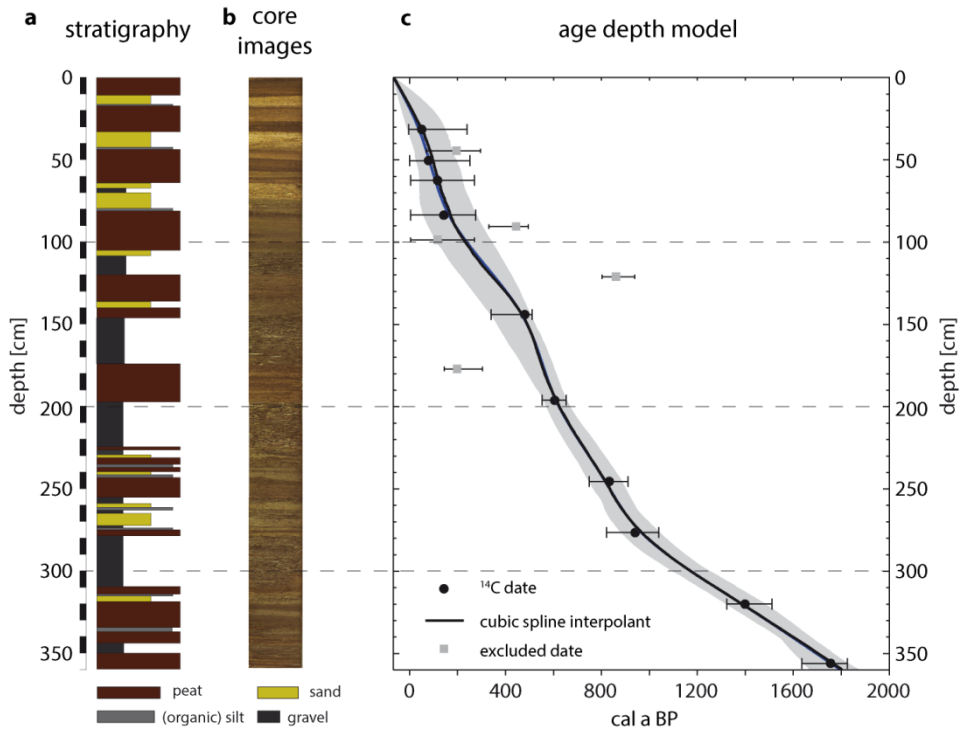

Figure 3. Stratigraphy and chronology of core C1581 of LP. (a) Schematic stratigraphy differentiated between peat (brown), (organic-) silt (light grey), sand (yellow) and gravel (dark grey), (b) color images and (c) age-depth-model based on ten ^{14}C dates (black dots with error bars) with a cubic spline interpolation with respective uncertainty band of (2σ) in grey (based on Kock et al., accepted). Also shown are radiocarbon dates excluded from the age-depth model (grey dots).

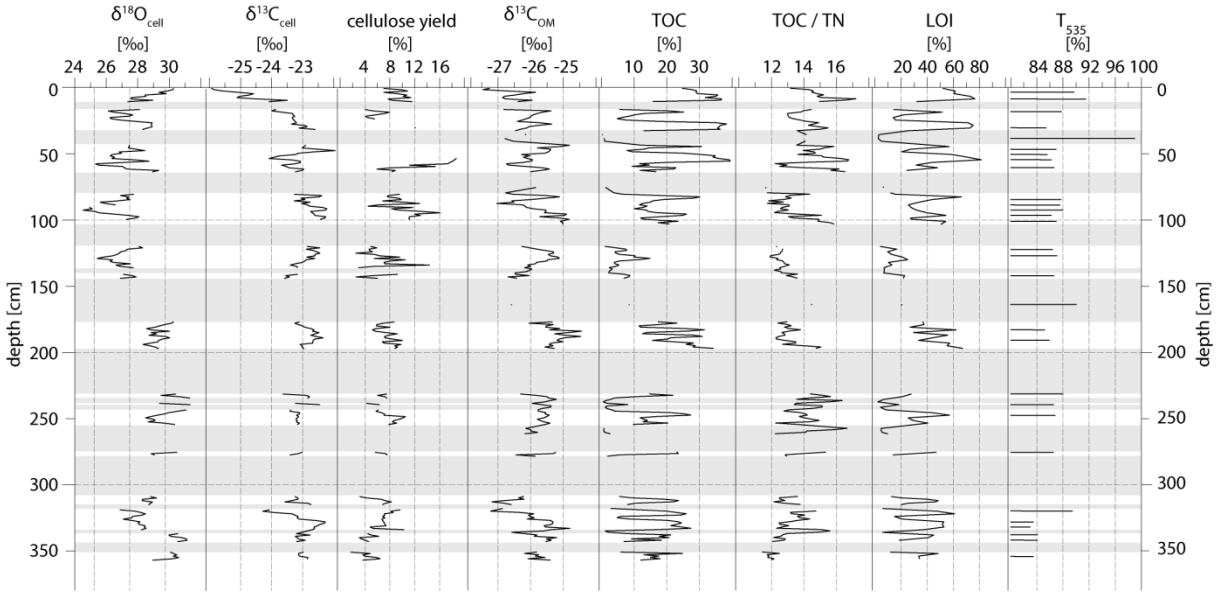

Figure 4. LP stable isotope composition of cellulose (fraction 200-1000 µm) as well as stable isotope and element composition of bulk material. Given are $\delta^{18}O_{cell}$ vs. VSMOW [‰], $\delta^{13}C_{cell}$ vs. VPDB [‰] and the cellulose yield of the extracted cellulose, $\delta^{13}C_{OM}$ vs. VPDB [‰], TOC [%], TN [%] values as well as the TOC/TN ratio, LOI and humification index (T_{535}) of the bulk material. Grey bars indicate gaps in the series caused by clastic layers (see stratigraphy in Figure 2a). Single missing values were caused by insufficient cellulose yield for analyses.

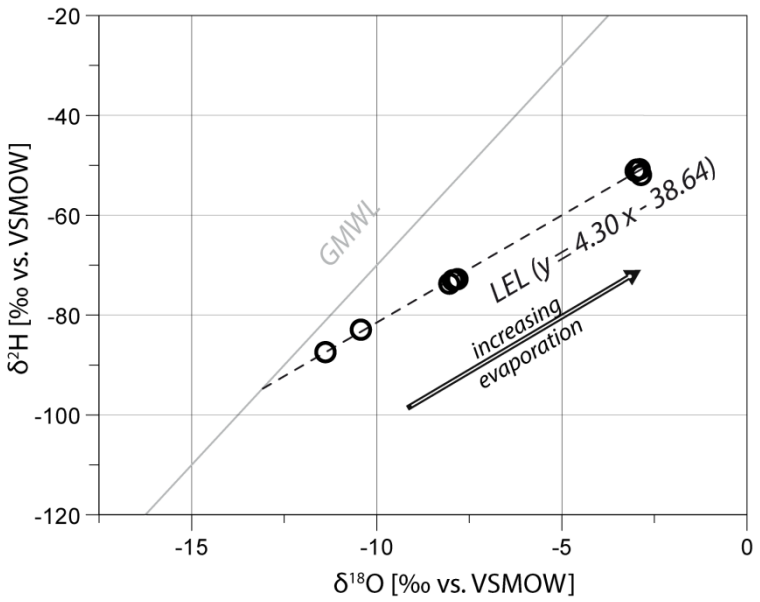

Figure 5. Isotopic composition of LP modern water samples from March 2016 (black circles) with their respective standard deviations included in the circle size (see Table S2). Also shown are the GMWL (black, $\delta^2H=8\delta^{18}O+10$) and the LEL (grey, $\delta^2H=4.30\delta^{18}O-38.64$). The intercept between GMWL and the LEL is an estimate for the isotopic composition of the meteoric water source.

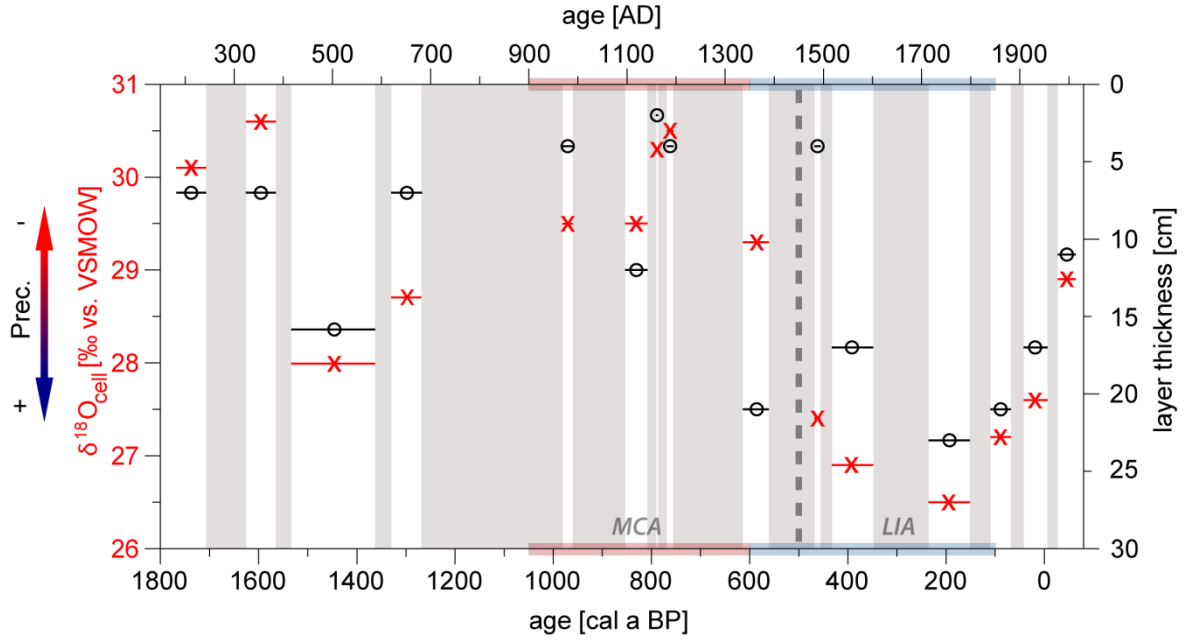

Figure 6. Mean oxygen isotope composition of cellulose (red crosses) and layer thickness (black circles, reverse scaled) of the peat sections of LP. Horizontal lines illustrate the temporal extension of the respective peat section. Grey bars indicate phases of clastic sediment accumulation. The transition towards more humid conditions after 500 cal a BP is illustrated by the dashed line. The period of the Medieval Climate Anomaly (MCA) is illustrated in red, while the Little Ice Age (LIA) is highlighted in blue.

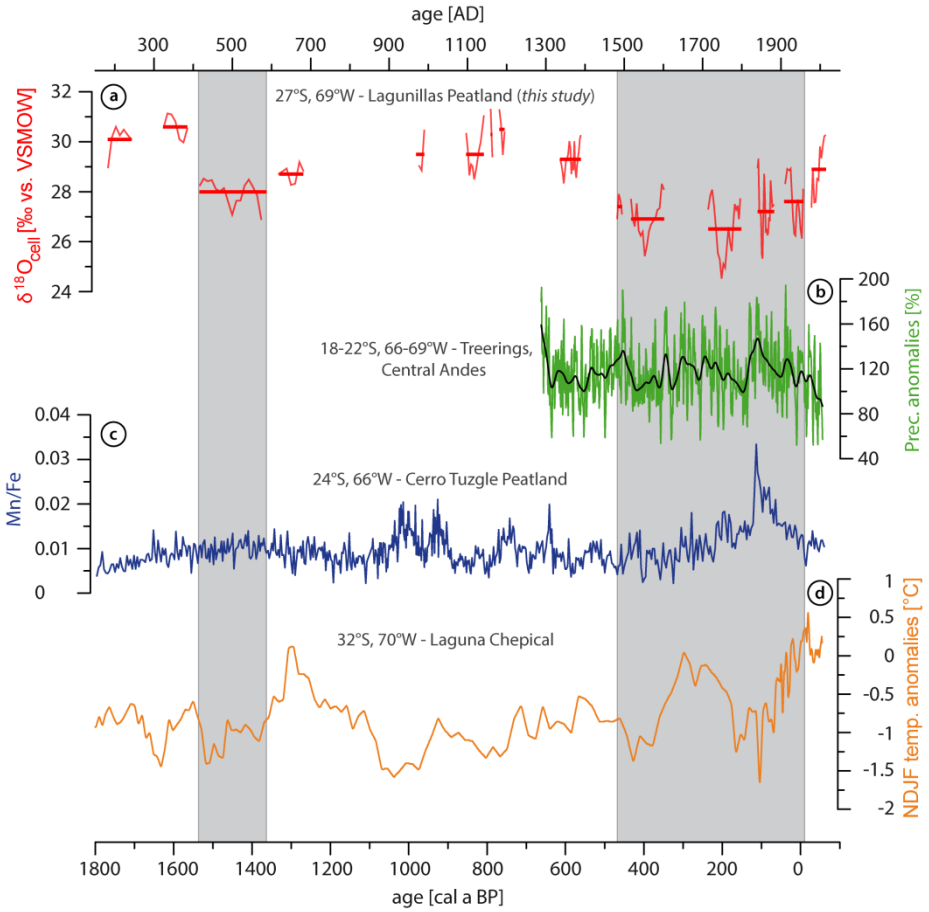

Figure 7. Regional paleoclimate comparison with the LP record. (a) $\delta^{18}O_{cell}$ vs. VSMOW of LP (red bars indicate mean oxygen isotope composition of the respective peat section). (b) Precipitation anomalies for the Central Andes based on *Polylepis tarapacana* tree rings (black line: 35 a spline; Morales *et al.*, 2012). (c) Mn/Fe values of the Cerro Tuzgle Peatland (Schittek *et al.*, 2016), presented on an updated age depth model recalculated with the SHCal13. (d) Austral summer temperature anomalies as recorded in the Laguna Chepical (de Jong *et al.*, 2013). Grey bars indicate the periods with increased humidity in LP.

Supplementary information – Kock *et al*. (2018)

Late Holocene environmental changes reconstructed from stable isotope and geochemical records from a cushion-plant peatland in the Chilean Central Andes (27°S)

Supplementary information to 'study area':

High-altitude cushion-plant peatlands are a typical, azonal unit of the high-Andean vegetation belt, occurring in the Central Andes between 3800 and 5000 m a.s.l. (Schittek *et al*., 2012; Ruthsatz, 1977). The floral composition of cushion peatlands is mainly dominated by Juncaceae like *Oxychloe*, *Distichia* and *Patosia*, frequently supplemented by Cyperaceae like *Phylloscirpus* or *Zameioscirpus* (Ruthsatz, 2008). These soligenous peatlands can develop on inclined slopes below springs, in shallow valley bottoms, below groundwater seepages in the lower part of fluvio-glacial debris fans and along the shores of high-altitude lakes (Schittek, 2014). Due to the harsh environmental conditions in the high Andes, with low temperatures, high solar radiation and decreased total atmospheric pressure (Körner, 2007), their morphological adaptations like cushion-growth and enrolled leaves, increase the resistance to water fluctuations, reduce evaporative water loss and protect the plants from high wind speeds (Schittek *et al*., 2016).

References (not listed references can be found in the manuscript):

Ruthsatz B. 1977. Pflanzengesellschaften und ihre Lebensbedingungen in den Andinen Halbwüsten Nordwest-Argentiniens. Dissertationes Botanicae 39, J. Cramer in der Gebrüder Borntraeger Verlagsbuchhandlung: Stuttgart.

Ruthsatz B. 2008. Hartpolstermoore der Hochanden NW-Argentiniens als Indikatoren für Klimagradienten, in Flora, Vegetation und Naturschutz zwischen Schleswig-Holstein und Südamerika, Festschrift für Klaus Dierßen zum 60. Geburtstag, Dengler J, Dolnik C, Trempel M (eds.). Mitteilungen der Arbeitsgemeinschaft für Geobotanik in Schleswig-Holstein und Hamburg 65: Hamburg; 209–238.

Supplementary information 'methods':

Various tests with 5% HCl proved that decarbonisation was not necessary for the determination of organic carbon content and for $\delta^{13}C_{OM}$ measurements, thus, the TC content is an equivalent of the total organic carbon content (TOC) (see Schittek et al., 2016 for further details).

Standards, including the International Atomic Energy Agency (IAEA) standard IAEA-CH6 cellulose powder ($\delta^{18}O$=37.09±0.09‰), two further commercially available cellulose powders, Merk ($\delta^{18}O$=29.97±0.08‰) and Fluka cellulose ($\delta^{18}O$=28.84±0.12‰), and two in-house standards, Rice ($\delta^{18}O$=23.64±0.15‰) and Peanut cellulose ($\delta^{18}O$ = 23.93‰±0.11‰), were calibrated against the reference standards IAEA-601 ($\delta^{18}O$ = 23.14‰) and IAEA-602 ($\delta^{18}O$ = 71.28‰).

Table S1. Radiocarbon ages of core C1581 from the LP. Samples belong to distinct peat sections further characterized in Table 2. Calibrated ages (2 σ) were calculated using CALIB 7.0.4 (Stuiver *et al*., 2013) and the SHCal13 data set (Hogg *et al*., 2013). MCAgeDepth ages are given as median values. Italic written samples were excluded from the age-depth-model. Additional, TOC values are given for the respective section. Additionally, the radiocarbon age of the extinct peat sample of the vertical incision is shown with its respective pMC amount and the calibrated age of CALIBomb (Reimer *et al*., 2004, available at http://calib.qub.ac.uk/CALIBomb/frameset.html). The table is supplemented on the base of Kock *et al*. (accepted).

peat section	core depth [cm]	profile depth [cm]	lab. no.	radiocarbon age [^{14}C a BP ± 1σ]	δ^{13}C [‰]	TOC [%]	cal. 2σ min. age [cal a BP]	cal. 2σ max. age [cal a BP]	MC Age Depth age [cal a BP]
2	31-32	31-32	Poz-83045	65 ± 30	-32.3	36.3	-6	241	51
3	*44-45*	*44-45*	*Poz-83046*	*225* ± 30	*-29.1*	*30.7*	*0*	*305*	*195*
3	50-51	50-51	Poz-91321	105 ± 30	-24.4	30.4	-3	253	79
3	62-63	62-63	Poz-83047	165 ± 30	-36.5	11.8	-2	278	116
4	83-84	83-84	Poz-83048	175 ± 35	-40.0	28.3	-1	281	142
4	*90-91*	*90-91*	*Poz-91323*	*410 ± 30*	*-28.6*	*12.7*	*325*	*499*	*444*
4	*98-99*	*98-99*	*Poz-83050*	*165 ± 30*	*-36.4*	*12.0*	-2	*278*	*116*
5	*123-124*	*120.5-121.5*	*Poz-83051*	*1020 ± 30*	*-40.0*	*/*	*799*	*933*	*861*
6	146-147	143.5-144.5	Poz-83052	450 ± 30	-41.7	6.9	333	516	480
7	*179-180*	*176.5-177.5*	*Poz-83053*	*240 ± 30*	*-34.7*	*17.5*	*145*	*309*	*199*
7	198-199	195.5-196.5	Poz-83054	660 ± 30	-32.6	28.0	552	651	605
10	254-255	245-246	Poz-83055	955 ± 30	-35.1	20.6	750	913	832
11	285-286	276-277	Poz-83056	1075 ± 35	-34.6	23.5	810	1050	940
12	362-363	319.5-320.5	Poz-83057	1560 ± 35	-31.4	19.9	1319	1511	1398
14	398-399	355.5-356.5	Poz-83058	1860 ± 30	-39.0	17.9	1628	1830	1756
/	*peat incision*		*Poz-83140*	*pMC:102.44 ± 0.32*			*-7.48*	*-6.23*	*/*

Table S2. Stable isotope values of modern water samples from the LP. Samples were collected in March 2016 from two different locations. LLA = Laguna Lagunillas, SW = stream water close to the coring site, LP = upper part of the Lagunillas Peatland, LP S = Lagunillas Peatland spring water sample.

sample ID	coordinates	location	altitude [m a.s.l.]	$\delta^{18}O$ vs. VSMOW [‰]	$\delta^{2}H$ vs. VSMOW [‰]
LLA 1	S 27°12'00.3" W 69°13'11.1"	lake water	4072	-2.86	-51.90
LLA 2	S 27°12'00.9" W 69°13'09.3"	lake water	4072	-3.01	-51.11
LLA 3	S 27°11'58.9" W 69°13'09.2"	lake water	4072	-2.90	-50.75
LLA 4	S 27°11'58.7" W 69°13'11.5"	lake water	4072	-2.97	-50.82
SW	S 27°12'04.2" W 69°17'13.5"	stream	3822	-10.43	-82.90
LP 1	S 27°11'54.3" W 69°13'32.7"	interspersed pool	4044	-7.87	-73.01
LP 2	S 27°11'54.2" W 69°13'32.8"	interspersed pool	4048	-8.04	-73.68
LP 3	S 27°11'54.4" W 69°13'32.8"	interspersed pool	4047	-7.94	-73.00
LP 4	S 27°11'54.4" W 69°13'32.9"	open water	4048	-7.84	-72.53
LP S1	S 27°12'02.4" W 69°14'58.7"	spring water	3979	-11.38	-87.40

Table S3. Pearson correlation coefficients (r) between geochemical and isotopic proxies of core C1581 (min. n=32). Correlated are humification index (T_{535}), total organic carbon (TOC) and nitrogen (TN) content and the TOC/TN ratio, loss on ignition (LOI), carbon and nitrogen isotopic composition of OM ($\delta^{13}C_{OM}$ $\delta^{15}N_{OM}$), oxygen and carbon isotope composition of cellulose of the size fraction 200-1000 µm ($\delta^{18}O_{cell}$, $\delta^{13}C_{cell}$) and the cellulose yield (yield). Significant correlations with a confidence interval of 95% ($p < 0.05$) are marked with *.

		OM							**cell 200-1000 µm**		
		T_{535}	**TOC**	**LOI**	**$\delta^{13}C$**	**TN**	**$\delta^{15}N$**	**TOC/TN**	**$\delta^{18}O$**	**$\delta^{13}C$**	**yield**
OM	**T_{535}**		-0.30	-0.32	-0.59*	-0.17	-0.24	0.47*	-0.21	-0.66*	0.37
	TOC	-0.30		0.99*	0.12	0.99*	-0.09	0.26*	0.14	-0.26*	0.31*
	LOI	-0.32	0.99*		0.16	0.98*	-0.09	0.18	0.13	-0.25*	0.23
	$\delta^{13}C$	-0.59*	0.12	0.16		0.14	-0.01	-0.08	0.12	0.63*	-0.13
	TN	-0.17	0.99*	0.98*	0.14		-0.06	0.12	0.16	-0.20*	0.26*
	$\delta^{15}N$	-0.24	-0.09	-0.09	-0.01	-0.06		-0.22*	-0.25*	0.32*	-0.02
	TOC/TN	0.47*	0.26*	0.18	-0.08	0.12	-0.22*		0.04	-0.33*	0.30*
cell 200-1000 µm	**$\delta^{18}O$**	-0.21	0.14	0.13	0.12	0.16	-0.25*	0.04		-0.11	-0.36*
	$\delta^{13}C$	-0.66*	-0.26*	-0.25*	0.63*	-0.20*	0.32*	-0.33*	-0.11		-0.12
	yield	0.37	0.31*	0.23	-0.13	0.26*	-0.02	0.30*	-0.36*	-0.12	